

UNIVERSITY OF PATRAS - SCHOOL OF ENGINEERING
DEPARTMENT OF ELECTRICAL AND COMPUTER ENGINEERING



**ΠΑΝΕΠΙΣΤΗΜΙΟ
ΠΑΤΡΩΝ**
UNIVERSITY OF PATRAS

DIVISION: SYSTEMS AND AUTOMATIC CONTROL

THESIS

of the student of the Department of Electrical and Computer Engineering of the School of
Engineering of the University of Patras

KARADIMOS ALEXIOS OF LOUKAS

STUDENT NUMBER: 1046820

Subject

**Robotic surgical tool manipulator - Recognition,
control and manipulation of laparoscopic tools**

Supervisor

Associate Professor Dr. Evangelos Dermatas

Co-Supervisor

Professor Dr. Anthony Tzes

Thesis Number:

Patras, 2020

ΠΙΣΤΟΠΟΙΗΣΗ

Πιστοποιείται ότι η διπλωματική εργασία με θέμα

Robotic surgical tool manipulator - Recognition, control and manipulation of laparoscopic tools

του φοιτητή του Τμήματος Ηλεκτρολόγων Μηχανικών και Τεχνολογίας Υπολογιστών

Karadimos Alexios of Loukas

(A.M.: 1046820)

παρουσιάστηκε δημόσια και εξετάστηκε στο τμήμα Ηλεκτρολόγων Μηχανικών και Τεχνολογίας Υπολογιστών στις

— / — / —

Ο Επιβλέπων

Ο Διευθυντής του Τομέα

Evangelos Dermatas
Associate Professor Dr.

Kazakos Demosthenes
Assistant Professor Dr.

CERTIFICATION

It is certified that the Thesis with Subject

Robotic surgical tool manipulator - Recognition, control and manipulation of laparoscopic tools

of the student of the Department of Electrical and Computer Engineering

Karadimos Alexios of Loukas

(R.N.: 1046820)

Was presented publicly and defended at the Department of Electrical and Computer
Engineering at

— / — / —

The supervisor

The Director of the Division

Evangelos Dermatas
Associate Professor Dr.

Kazakos Demosthenes
Assistant Professor Dr.

Thesis details

Subject: **Robotic surgical tool manipulator - Recognition, control and manipulation of laparoscopic tools**

Student: **Karadimos Alexios of Loukas**

Supervising Team:

Associate Professor Dr. Evangelos Dermatas, University of Patras
Professor Dr. Anthony Tzes, NYU Abu Dhabi

Thesis research period:

Abstract

Sunt proident ut incidunt veniam ad excepteur aute nostrud. Anim nulla magna proident dolore non laboris deserunt irure. Aliqua velit quis labore quis nisi. Adipisicing amet dolor officia est ex nulla enim anim minim laboris nisi adipisicing cupidatat. Ut do consequat est ad sint dolore. Eiusmod ipsum nulla do aute culpa ad veniam eu in sunt qui laboris. Ea exercitation et quis fugiat.

Περίληψη

Sunt proident ut incidunt veniam ad excepteur aute nostrud. Anim nulla magna proident dolore non laboris deserunt irure. Aliqua velit quis labore quis nisi. Adipisicing amet dolor officia est ex nulla enim anim minim laboris nisi adipisicing cupidatat. Ut do consequat est ad sint dolore. Eiusmod ipsum nulla do aute culpa ad veniam eu in sunt qui laboris. Ea exercitation et quis fugiat.

Acknowledgements

Sunt proident ut incidunt veniam ad excepteur aute nostrud. Anim nulla magna proident dolore non laboris deserunt irure. Aliqua velit quis labore quis nisi. Adipisicing amet dolor officia est ex nulla enim anim minim laboris nisi adipisicing cupidatat. Ut do consequat est ad sint dolore. Eiusmod ipsum nulla do aute culpa ad veniam eu in sunt qui laboris. Ea exercitation et quis fugiat.

Contents

1 Introduction	10
1.1 Surgery Robotics	10
1.2 Bibliography Overview	13
1.3 Methodology & Approach	13
2 Robotic arm Kinematic Analysis	13
2.1 Robotic arm, DH parameters & Forward Kinematics	13
2.2 Inverse Kinematics	14
2.2.1 Decoupling Technique	14
2.2.2 Workspace constraints & Singularity points	15
2.2.3 Solutions for 7DoF numerically	15
2.2.4 Comparison of Inverse Kinematics Techniques	16
3 Grasping	16
3.1 Gripper & Forward Kinematics	16
3.2 Gripper Inverse Kinematics	16
3.3 Force closure	17
3.4 Firm grasping algorithm & Force control	17
4 Scene and object recognition with Computer Vision	17
4.1 Laparoscopic tool detection	17
4.2 Stereoscopic vision	18
4.3 Calculation of tool position and orientation	18
4.4 Calculation of grasping points	19
4.5 Trocar detection & Estimation of fulcrum point	19
5 Laparoscopic tool manipulation	20
5.1 Tool pose	20
5.2 Pivoting motion with respect to Fulcrum Point	21
5.2.1 Circular trajectory of tool tip	21
5.2.2 Circular arc trajectory of tool tip	22
5.2.3 Line segment trajectory of tool tip	22
5.3 Task space analysis	22
6 Path Planning	23
6.1 Path searching	23
6.2 Pick and place algorithm	23
7 Trajectory Planning	23
7.1 Trajectory planning in cartesian coordinates	23
7.2 Trajectory planning in joint angles space	24
8 Implementation with the ROS framework	25
8.1 Gazebo simulation environment	25
8.2 Visualization and Motion Planning with RViz and Moveit	25
8.3 Experiments and Development methodology	26
8.3.1 Robot Planner 1	26
8.3.2 Robot Planner 2	26
8.3.3 Robot Planner 3	26
8.3.4 Robot Planner 4	26
8.3.5 Robot Planner 5	26

9 Results and Future Work	26
9.1 Results	26
9.2 Conclusions & Comparison with similar projects	26
9.3 Future Work	26
Nomenclature	27
List of Figures	29
List of programs	29
Bibliography	29

1 Introduction

1.1 Surgery Robotics

Surgery Robotics is a field of Surgery where the surgeon operates on the patient via a computer, specialised equipment and robotic arms, to which the surgical tools needed for the operation are attached. According to surgical bibliography, robotics and laparoscopic procedures are used in general surgery, cardiothoracic surgeries, colon surgeries, gynecology, neurosurgery and orthopedics.

Robotic mechanisms were first introduced in Medicine, in 1987 with the first laparoscopic surgery of a cholecystectomy. Since then numerous laparoscopic operations have been performed and there has been a lot of improvements and innovations in this field. Such surgical operations are characterised as **minimally invasive**, because the surgical incisions made at the patient are very small and thus the probability of infection of the patient during or after the operation are very small, the hospitalization time is reduced (which means mean better and more efficient use of hospital resources) and the overall recovery of the patient is significantly faster and less painful.

However, traditional laparoscopic mechanisms have some downsides as well. First of all, the surgeon should operate in a mirrored-way, meaning that they should move at the opposite direction from what they saw at the screen (this effect is also known as the **fulcrum effect**), in order to reach the desired point of operation. Earlier laparoscopic tools had less degrees of freedom, which means less flexibility in motion control. Moreover these systems provided limited touch sensibility and feedback to the doctor they were very susceptible to the surgeon's micro movements and tremble.

The first application of robotics in Surgery appears in 1985, when Kwoh et al. [26] used a **PUMA 560**, a standard industrial robotic arm, to perform a neurosurgical biopsy, where the biopsy needle was inserted in the brain and guided with the help of Computed Tomography. This successful application was followed by the **PROBOT** surgical robot [20], which was developed at the Imperial College and used in a prostatectomy operation. Another example of an early surgery robot was the **ROBODOC** system [4] developed by Integrated Surgical Supplies in Sacramento California, which was the first to be used in orthopedics for a hip replacement surgery and was also the first to be approved by the FDA (Food & Drug Administration, organization responsible for medical devices, drugs etc.).



Figure 1: The PUMA 560 robotic arm, which was the first to be used in surgery robotics in 1985

Some other important surgery robots are listed below:

- **AESOP®Endoscope Positioner**
- **HERMES®Control Center**
- **daVinci Surgical System®**

- **SOCRATES Robotic Telecollaboration System**
- **Raven-II [13]**: An open platform for collaborative research on surgical robotics.



Figure 2: DaVinci Xi Patient Cart

Surgical robotics have a huge impact in Medicine and Healthcare in general. Some of the advantages are the following:

- **Minimally Invasive Procedures** which means
 - Smaller incisions
 - Less blood loss
 - Reduced risk of inpatient infection
 - Less pain
 - Faster patient recovery
- Increased precision and reduced human errors
 - Smooth and precise movements
 - Detection and correction of errors caused by hand tremble
- No fulcrum effect and intuitive manipulation of surgical tools
- Haptic feedback

- Teleoperation (currently in the same room only): the surgeon operates while they sit on a special ergonomic console, which makes the long procedures more comfortable and efficient.



Figure 3: DaVinci Xi Surgeon Console

1.2 Bibliography Overview

1.3 Methodology & Approach

2 Robotic arm Kinematic Analysis

2.1 Robotic arm, DH parameters & Forward Kinematics

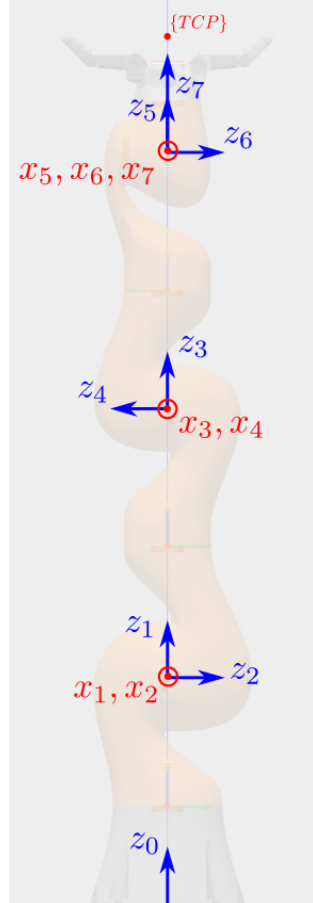


Figure 4: Joint reference frames of the KUKA iiwa14 robot

i	θ_i (rad)	L_{i-1} (m)	d_i (m)	α_{i-1} (rad)
1	θ_1	0	0.36	0
2	θ_2	0	0	$-\pi/2$
3	θ_3	0	0.36	$\pi/2$
4	θ_4	0	0	$\pi/2$
5	θ_5	0	0.4	$-\pi/2$
6	θ_6	0	0	$-\pi/2$
7	θ_7	0	0	$\pi/2$

$${}^{i-1}T_i = \begin{bmatrix} c\theta_i & -s\theta_i & 0 & L_{i-1} \\ s\theta_i c a_{i-1} & c\theta_i c a_{i-1} & -s a_{i-1} & -s a_{i-1} d_i \\ s\theta_i s a_{i-1} & c\theta_i s a_{i-1} & c a_{i-1} & c a_{i-1} d_i \\ 0 & 0 & 0 & 1 \end{bmatrix}$$

2.2 Inverse Kinematics

2.2.1 Decoupling Technique

In this section the inverse kinematics problem is solved for only the 6 out of the 7 total degrees of freedom. The third joint is not used in this analysis and its angle is set to zero $\theta_3 = 0$. The rest of the joints form a special kind of kinematic chain that can be solved using the decoupling technique. In this technique the Inverse kinematics problem is split to 2 separate subproblems, one for the position and one for the orientation of the end-effector. This technique can be applied in this case because the axes of the 3 last joints intersect at the same point and they form an Euler wrist.

To solve for the joints' angles, the transformation matrix 0T_7 of the end-effector with respect to the robot's base is required. Usually the transformation ${}^U T_{tcp}$ is known, which is the pose of Tool's center point (TCP) with respect to the Universal Coordinate Frame $\{U\}$ from which the required 0T_7 can be calculated

$$\begin{aligned} {}^U T_{tcp} &= {}^U T_0 \ {}^0 T_7 \ {}^7 T_{tcp} \\ {}^0 T_7 &= {}^U T_0^{-1} \ {}^U T_{tcp} \ {}^7 T_{tcp}^{-1} \\ {}^0 T_7 &= \begin{bmatrix} R_t & \mathbf{p}_t \\ 0 & 1 \end{bmatrix} \end{aligned}$$

where ${}^U T_0$, ${}^7 T_{tcp}$ are translation transformations by a constant distance and R_t , \mathbf{p}_t are the target's orientation and position respectively.

$$\begin{aligned} {}^0 \mathbf{p}_5 &= {}^0 T_4 {}^4 \mathbf{p}_5 = \begin{bmatrix} p_x \\ p_y \\ p_z \end{bmatrix} \\ \theta_1 &= \begin{cases} \text{atan2}(p_y, p_x) \\ \pi - \text{atan2}(p_y, p_x) \end{cases} \quad (2.2.1) \end{aligned}$$

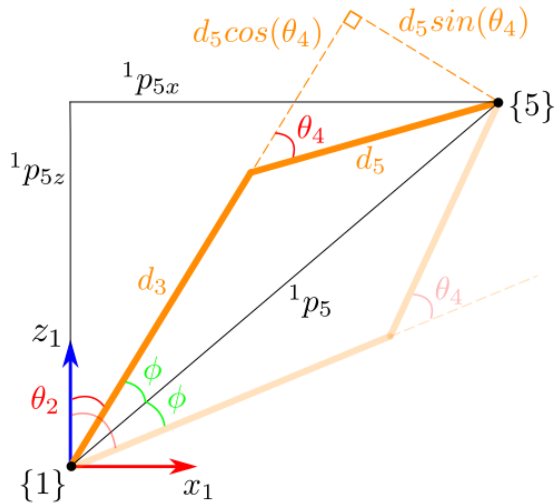


Figure 5: Calculation of angles θ_2, θ_4

$$\varphi = \arccos \left(\frac{d_3^2 + \|{}^1 p_5\|^2 - d_5^2}{2d_3\|{}^1 p_5\|} \right)$$

$$\theta_2 = \text{atan}2\left(\sqrt{p_x^2 + p_y^2}, {}^1p_{5z}\right) \pm \varphi \quad (2.2.2)$$

$$c_4 = \frac{\|{}^1p_5\|^2 - d_3^2 - d_5^2}{2d_3d_5}$$

$$\theta_4 = \text{atan}2\left(\pm\sqrt{1 - c_4^2}, c_4\right) \quad (2.2.3)$$

Once $\theta_1, \theta_2, \theta_3, \theta_4$ are known, the orientation matrix of the wrist can be calculated as following

$$R_{target} = \begin{bmatrix} i_x & j_x & k_x \\ i_y & j_y & k_y \\ i_z & j_z & k_z \end{bmatrix}$$

$$\theta_6 = \text{atan}2\left(\pm\sqrt{1 - k_y^2}, k_y\right) \quad (2.2.4)$$

$$\theta_7 = \text{atan}2(-j_y, i_y)$$

$$\theta_5 = \text{atan}2(-k_z, k_x)$$

2.2.2 Workspace constraints & Singularity points

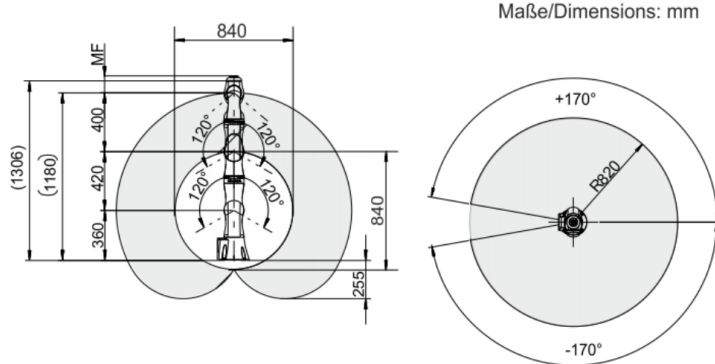


Figure 6: KUKA iiwa LBR14 workspace dimensions

Singularity points:

- When $p_x^2 + p_y^2 = 0$ then the end-effector lies on the z-axis and θ_1 is not defined
- When $\sin(\theta_6) = 0$ then the angles θ_5, θ_7 are not defined

2.2.3 Solutions for 7DoF numerically

Jacobian

$$J = J(\mathbf{q}) = [J_1, J_2, \dots, J_7] \in \mathbb{R}^{6 \times 7}$$

$$J_i = \begin{bmatrix} {}^0\mathbf{z}_i \times ({}^0\mathbf{p}_8 - {}^0\mathbf{p}_i) \\ {}^0\mathbf{z}_i \end{bmatrix} \quad (2.2.5)$$

$J(\mathbf{q})$ is non rectangular and thus non-invertible. Instead of the inverse of the Jacobian the pseudoinverse is calculated which by the equation

$$J^\dagger = J^\top (JJ^\top)^{-1} \quad (2.2.6)$$

2.2.4 Comparison of Inverse Kinematics Techniques

3 Grasping

3.1 Gripper & Forward Kinematics

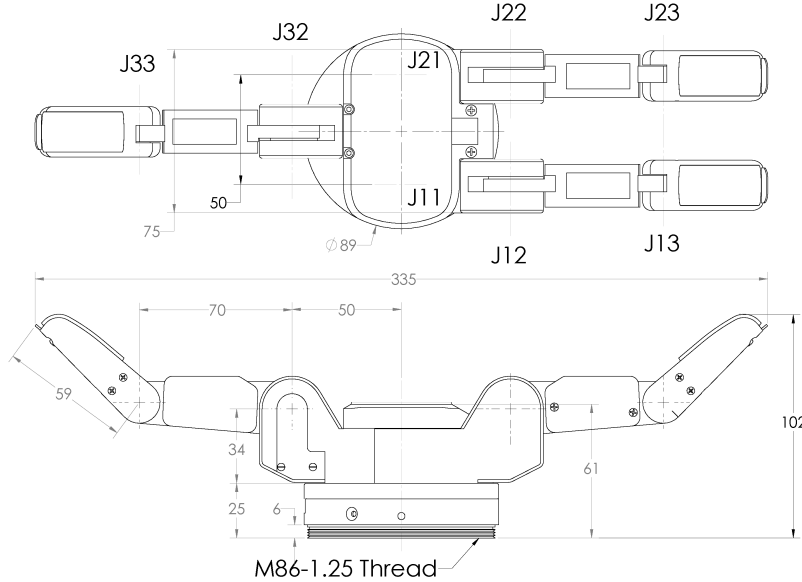


Figure 7: Barrett Hand gripper (model BH8-282) dimensions

3.2 Gripper Inverse Kinematics

The following Inverse Kinematics analysis refers to one finger of the Barrett Hand gripper, which has 3 revolute joints. Finger 3 has only 2 revolute joints for which the angle solutions are the same with the solutions of the last 2 joints of the other fingers. Let

$$\mathbf{p} = \begin{bmatrix} p_x \\ p_y \\ p_z \end{bmatrix}$$

be the position of the grasp point for one finger. The first angle can easily be calculated as

$$\varphi_1 = \text{atan2}(p_y, p_x) \quad (3.2.1)$$

Next, we calculate the third angle based on the law of cosines (see fig.)

$$\begin{aligned} \cos\left(\pi - \varphi_3 - \frac{\pi}{4}\right) &= \frac{L_2^2 + L_3^2 - p^2}{2L_2L_3} \\ \cos\left(\varphi_3 + \frac{\pi}{4}\right) &= \frac{p^2 - L_2^2 - L_3^2}{2L_2L_3} \\ \varphi_3 &= \text{atan2}\left[\pm\sqrt{1 - \left(\frac{p^2 - L_2^2 - L_3^2}{2L_2L_3}\right)^2}, \frac{p^2 - L_2^2 - L_3^2}{2L_2L_3}\right] - \frac{\pi}{4} \end{aligned} \quad (3.2.2)$$

In a more general case, the first argument of the *atan2* function in the expression of φ_3 could also be negative, but in this case this second solution is rejected, because due to mechanical constraints, this angle can't be negative. After having calculated φ_3 we can calculate φ_2

$$\begin{aligned}
 \tan(\psi + \varphi_2) &= \frac{p_z}{\sqrt{p_x^2 + p_y^2}} \\
 \tan(\psi) &= \frac{L_3 \sin(\varphi_3 + \frac{\pi}{4})}{L_2 + L_3 \cos(\varphi_3 + \frac{\pi}{4})} \\
 \varphi_2 &= \text{atan2}(p_z, \sqrt{p_x^2 + p_y^2}) - \text{atan2}\left[L_3 \sin\left(\varphi_3 + \frac{\pi}{4}\right), L_2 + L_3 \cos\left(\varphi_3 + \frac{\pi}{4}\right)\right]
 \end{aligned} \tag{3.2.3}$$

3.3 Force closure

The planar case, the spatial case & convex hull test.

3.4 Firm grasping algorithm & Force control

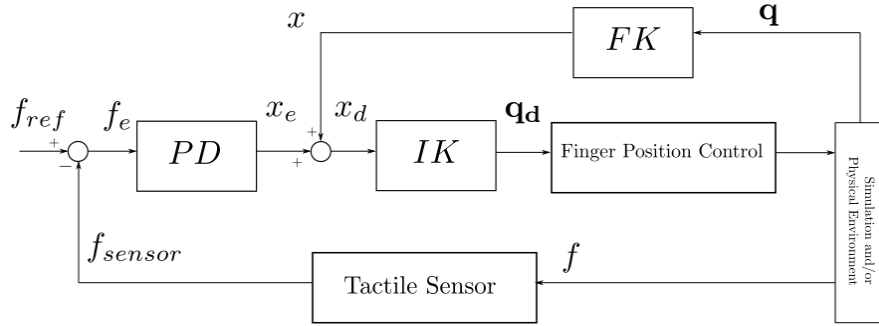


Figure 8: Force control on a Barrett Hand gripper finger

4 Scene and object recognition with Computer Vision

4.1 Laparoscopic tool detection

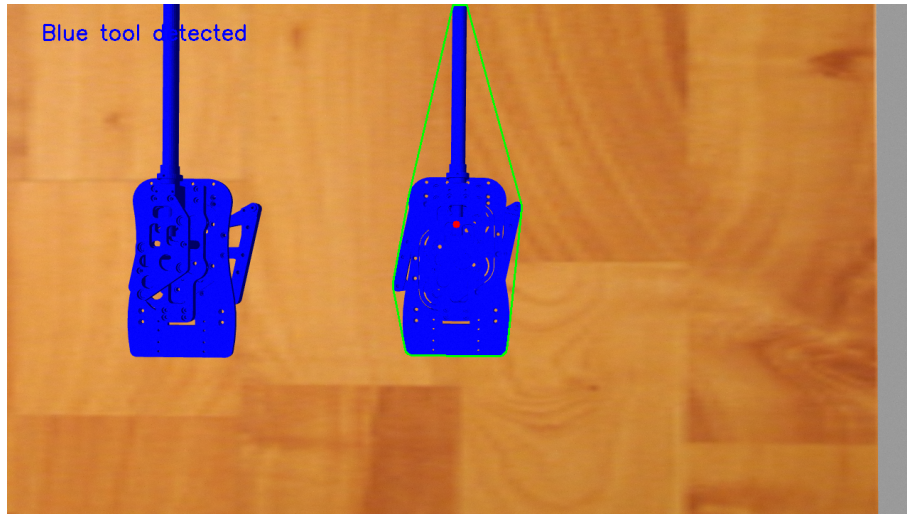


Figure 9: Simple tool detection in simulation based on color, using OpenCV. The green polygon is the convex hull, and the red point is the estimated center of mass

4.2 Stereoscopic vision

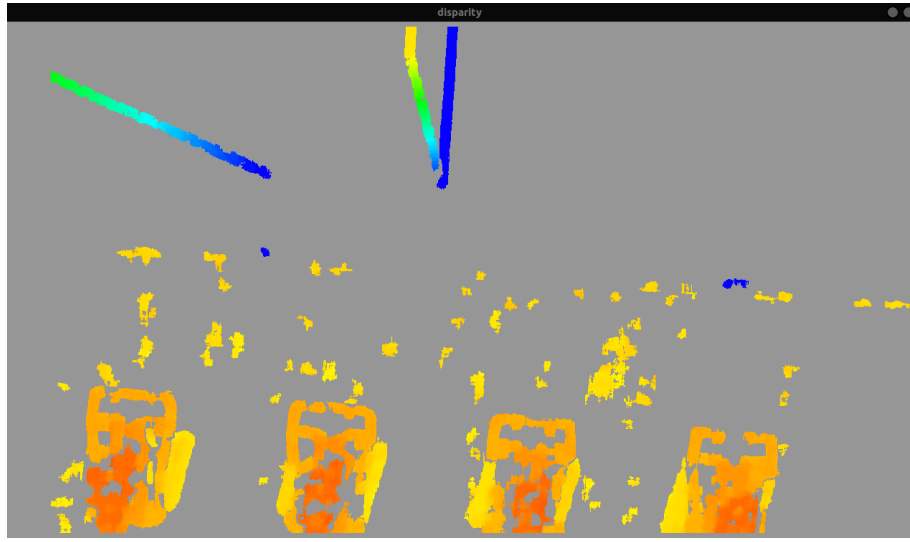


Figure 10: Disparity image calculated from the 2 cameras

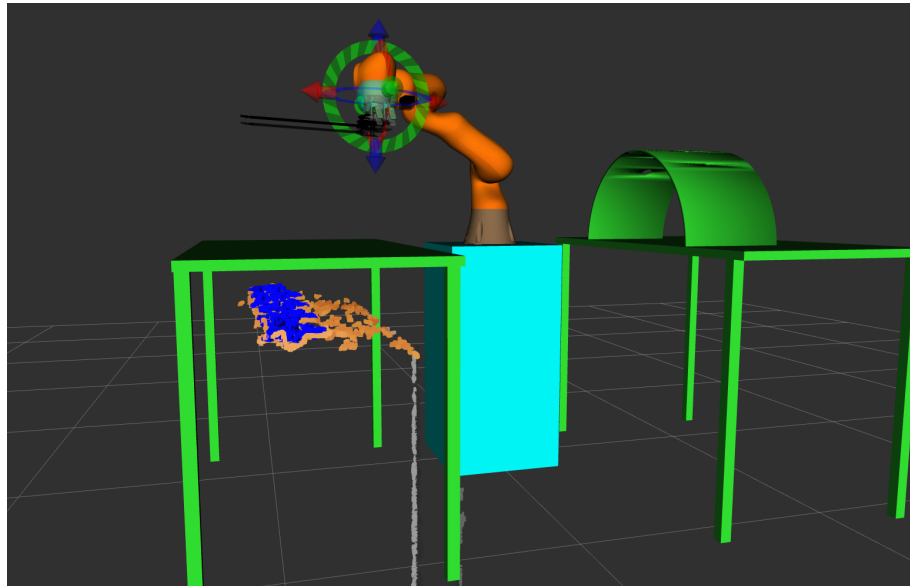


Figure 11: Point cloud of surgical tools, generated from the 2 cameras and visualized in RViz

4.3 Calculation of tool position and orientation

In order for the gripper to grasp correctly the laparoscopic tool, it is required to calculate the tool's position and orientation in the pixel space which must then be converted with respect to the robot's workspace. From all the pixels that have been classified as part of the laparoscopic tool, one can estimate the center of mass and two perpendicular vectors attached to that point that define the orientation. The center of mass is simply the average of the (x, y) coordinates of all the tool's pixels

$$(\bar{x}, \bar{y}) = \left(\frac{1}{N} \sum_{i=1}^N x_i, \frac{1}{N} \sum_{i=1}^N y_i \right)$$

The two orientation vectors are the eigenvectors of the covariance matrix of the above pixels. Let \mathbf{a}, \mathbf{b} be the orientation vectors, then \mathbf{a}, \mathbf{b} are solutions of the equation

$$C\mathbf{v} = \lambda\mathbf{v}$$

where C is the covariance matrix given by

$$C = \begin{bmatrix} \sigma(x, x) & \sigma(x, y) \\ \sigma(y, x) & \sigma(y, y) \end{bmatrix}$$

$$\sigma(x, y) = \frac{1}{n-1} \sum_{i=1}^N (x_i - \bar{x})(y_i - \bar{y})$$

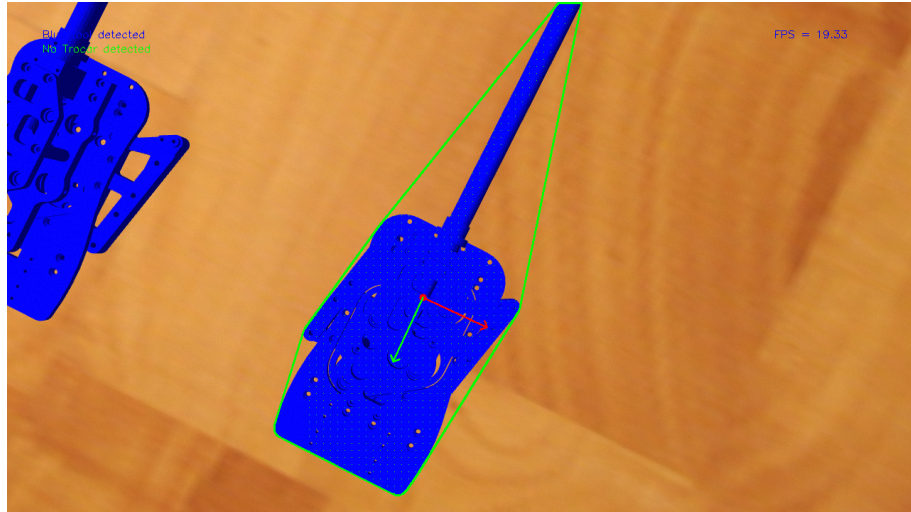


Figure 12: Estimation of tool's pose (position and orientation)

4.4 Calculation of grasping points

4.5 Trocar detection & Estimation of fulcrum point

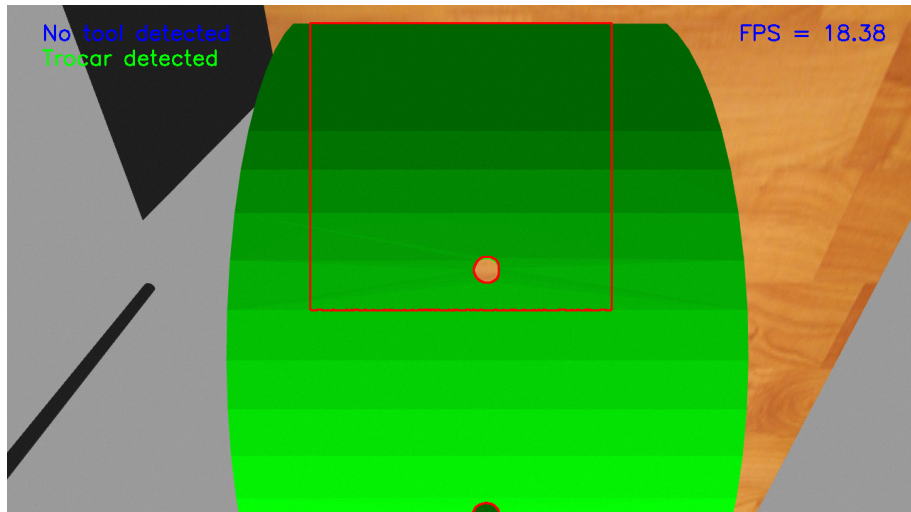


Figure 13: Simple trocar detection in simulation based on color, using OpenCV. In simulation, the trocar is simply considered to be a small cylindrical hole and it's center is the fulcrum point

5 Laparoscopic tool manipulation

5.1 Tool pose

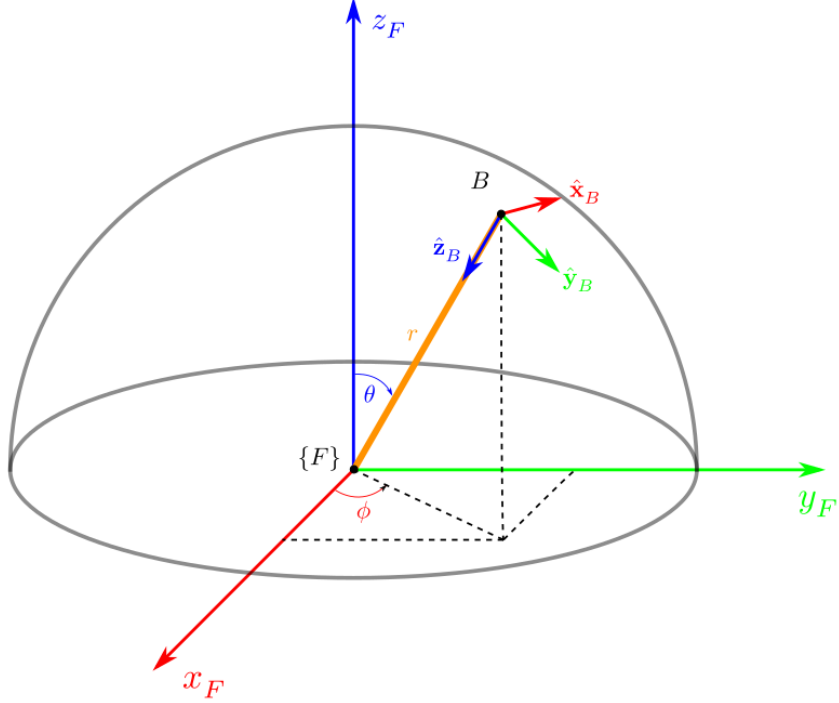


Figure 14: Tool pose at target point B calculated with respect to Fulcrum's reference frame $\{F\}$

The laparoscopic tool pose is given by the position and orientation vectors at target point B with respect to the coordinate frame $\{F\}$. The pose is given by the following transformation matrix

$${}^F T_B = \begin{bmatrix} {}^F R_B & {}^F \mathbf{p}_B \\ \mathbf{0} & 1 \end{bmatrix} \quad \text{where} \quad {}^F R_B = [\hat{\mathbf{x}}_B \quad \hat{\mathbf{y}}_B \quad \hat{\mathbf{z}}_B]$$

$$\hat{\mathbf{x}}_B = \hat{\theta} = \cos(\theta)\cos(\varphi)\hat{\mathbf{x}}_F + \cos(\theta)\sin(\varphi)\hat{\mathbf{y}}_F - \sin(\theta)\hat{\mathbf{z}}_F = \begin{bmatrix} \cos(\theta)\cos(\varphi) \\ \cos(\theta)\sin(\varphi) \\ -\sin(\theta) \end{bmatrix}$$

$$\hat{\mathbf{y}}_B = \hat{\varphi} = -\sin(\varphi)\hat{\mathbf{x}}_F + \cos(\varphi)\hat{\mathbf{y}}_F = \begin{bmatrix} -\sin(\varphi) \\ \cos(\varphi) \\ 0 \end{bmatrix}$$

$$\hat{\mathbf{z}}_B = -\hat{\mathbf{r}} = -(sin(\theta)\cos(\varphi)\hat{\mathbf{x}}_F + sin(\theta)\sin(\varphi)\hat{\mathbf{y}}_F + cos(\theta)\hat{\mathbf{z}}_F) = \begin{bmatrix} -\sin(\theta)\cos(\varphi) \\ -\sin(\theta)\sin(\varphi) \\ -\cos(\theta) \end{bmatrix}$$

The position of the point B is given in spherical coordinates by:

- $r = \rho$: outside penetration of laparoscopic tool
- $\theta = \beta$: altitude angle
- $\varphi = \alpha$: orientation angle

thus the position with respect to the coordinate frame $\{F\}$ is given by

$${}^F \mathbf{p}_B = \begin{bmatrix} \rho \sin(\beta) \cos(\alpha) \\ \rho \sin(\beta) \sin(\alpha) \\ \rho \cos(\beta) \end{bmatrix} = \rho \hat{\mathbf{r}}$$

The above goal point must be the same as the *TCP* point of the robot's end-effector. This means, that this pose must be converted with respect to the robot's reference frames.

$$\begin{aligned} {}^U T_{TCP} &= {}^U T_B \\ {}^U T_0 {}^0 T_7 {}^7 T_{TCP} &= {}^U T_F {}^F T_B \\ {}^0 T_7 &= {}^U T_0^{-1} {}^U T_F {}^F T_B {}^7 T_{TCP}^{-1} \end{aligned} \quad (5.1.1)$$

5.2 Pivoting motion with respect to Fulcrum Point

5.2.1 Circular trajectory of tool tip

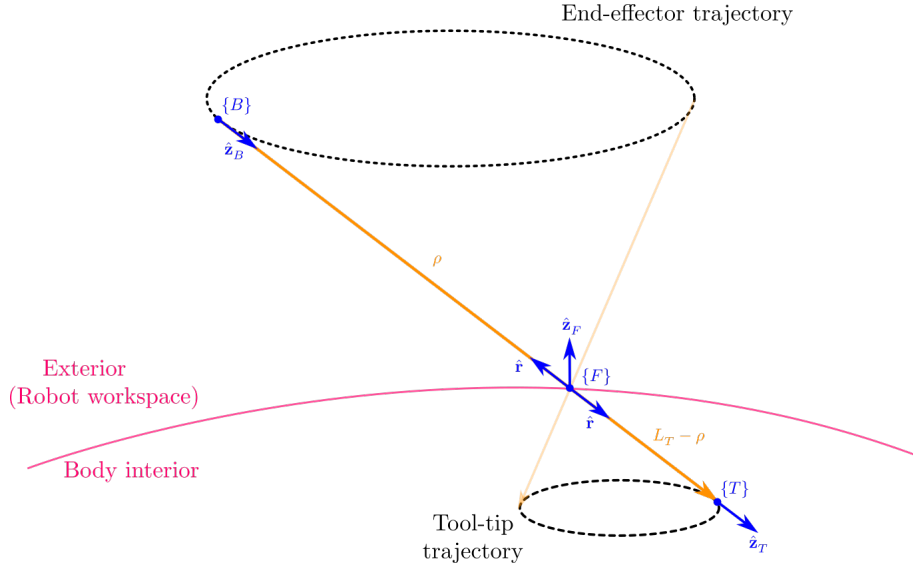


Figure 15: Circular trajectory of tool tip with respect to Fulcrum reference frame

To generate a circular trajectory for the pivot movement we must specify the center of the circle and a vector whose magnitude is the radius of the circle and it's direction gives the orientation of the plane that the circle lies at. The simplest case of a circular trajectory is the one, whose circle lies in a plane parallel to the xy plane.

We first consider the motion of the laparoscopic tool tip on a circle parallel to a z -plane, with respect to the $\{F\}$ coordinate frame.

$$(x_F - x_{F0})^2 + (y_F - y_{F0})^2 = r_0^2, \quad z_F = z_{F0}$$

It's often more convenient to express trajectories in a parametric form, which makes it easier to calculate all the waypoints of the trajectory

$$\begin{cases} x_F = r_0 \cos(2\pi t) + x_{F0} \\ y_F = r_0 \sin(2\pi t) + y_{F0} \\ z_F = z_{F0} \end{cases}, \quad t \in [0, 1]$$

After having calculated the cartesian coordinates we can calculate the spherical coordinates as follows

$$\begin{cases} r = \sqrt{x_F^2 + y_F^2 + z_F^2} \\ \theta = \text{atan2}\left(\sqrt{x_F^2 + y_F^2}, z_F\right) \\ \varphi = \text{atan2}(y_F, x_F) \end{cases} \quad (5.2.1)$$

5.2.2 Circular arc trajectory of tool tip

To generate a circular arc trajectory for a pivot motion we must specify the same parameters as in the circular trajectory as well as the length of the arc or the total angle of the arc section.

5.2.3 Line segment trajectory of tool tip

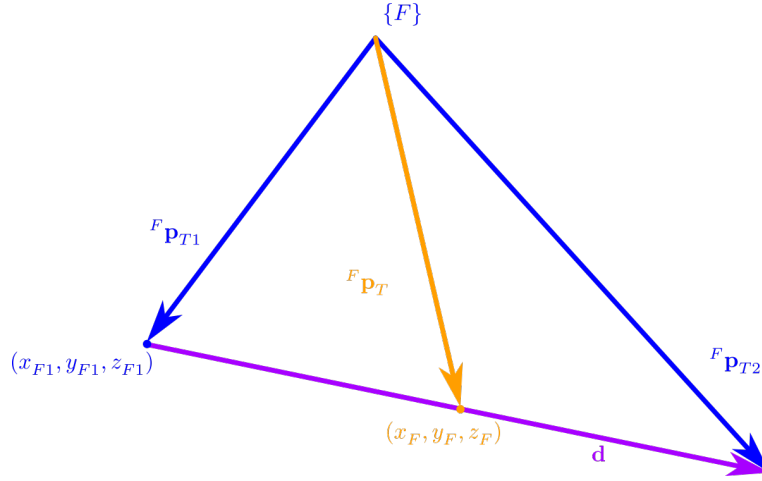


Figure 16: Line segment trajectory of tool tip with respect to Fulcrum reference frame

$$\begin{aligned} \mathbf{d} &= {}^F \mathbf{p}_{T2} - {}^F \mathbf{p}_{T1} = [l, m, n]^\top \\ {}^F \mathbf{p}_T &= [x_F, y_F, z_F]^\top \\ {}^F \mathbf{p}_T &= {}^F \mathbf{p}_{T1} + t \mathbf{d} \\ t &= \frac{x_F - x_{F1}}{l} = \frac{y_F - y_{F1}}{m} = \frac{z_F - z_{F1}}{n} \quad t \in [0, 1] \\ \begin{cases} x_F = tl + x_{F1} \\ y_F = tm + y_{F1} \\ z_F = tn + z_{F1} \end{cases} \end{aligned}$$

After having calculated the cartesian coordinates we can calculate the spherical coordinates using the 5.2.1 equations.

The line segment trajectory of tool tip, as analysed in this section needs no implementation as it is already implemented in the ROS MoveIt library and can be used by calling the method **computeCartesianPath**.

5.3 Task space analysis

Dexterity analysis for tool's task space

$$\mathcal{D} = \mathcal{L}_q \mathcal{M} \quad (5.3.1)$$

where

$$\mathcal{M} = \sqrt{\det(J J^\top)} \quad (5.3.2)$$

$$\mathcal{L}_q = 1 - \exp \left\{ -\kappa \prod_{i=1}^{n_k} \frac{(q_i - q_{i,\min})(q_{i,\max} - q_i)}{(q_{i,\max} - q_{i,\min})^2} \right\} \quad (5.3.3)$$

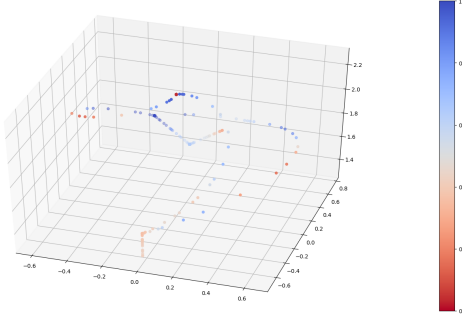


Figure 17: Plot the manipulability of the robot arm at sample points of the executed trajectory

For maximum dexterity at most points of a trajectory in a pivoting motion, the pivot sub- taskspace (i.e. the space of all configurations of feasible pivot motions) must be fully within the robot's whole reachable taskspace, otherwise only a small range of pivot movements will be feasible.

6 Path Planning

6.1 Path searching

Find path points (position and orientation) by avoiding collisions, asserting that path points is within robot's workspace and by avoiding singularity points.

6.2 Pick and place algorithm

7 Trajectory Planning

At this step, given the points of the desired path, a more detailed trajectory is calculated, which will contain all the waypoints that the robot will have to visit.

7.1 Trajectory planning in cartesian coordinates

Connect the points from path planning with line segments and add more points if needed

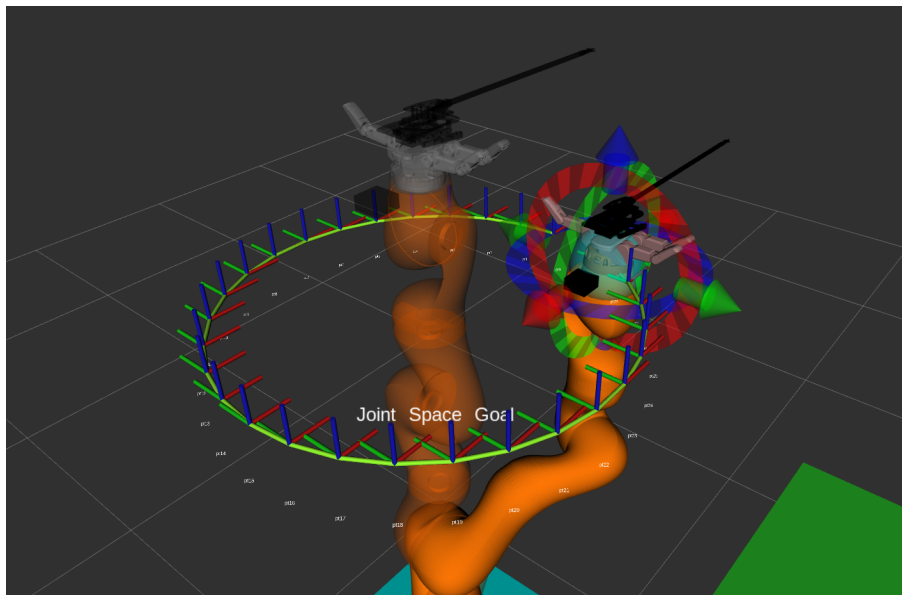


Figure 18: Circular trajectory around the z axis of the home position of the robot

It is very important that the designed trajectory respects the joints angles' range. For example depending on the starting position of the circular trajectory depicted at figure 18, the robot arm may reach it's joint bounds and in order to continue executing the trajectory it will have to make a sudden jump to reset the angles. This could have serious side-effects for both the surgical task and thus the patient, as well as for the operating staff, who control the robot.

7.2 Trajectory planning in joint angles space

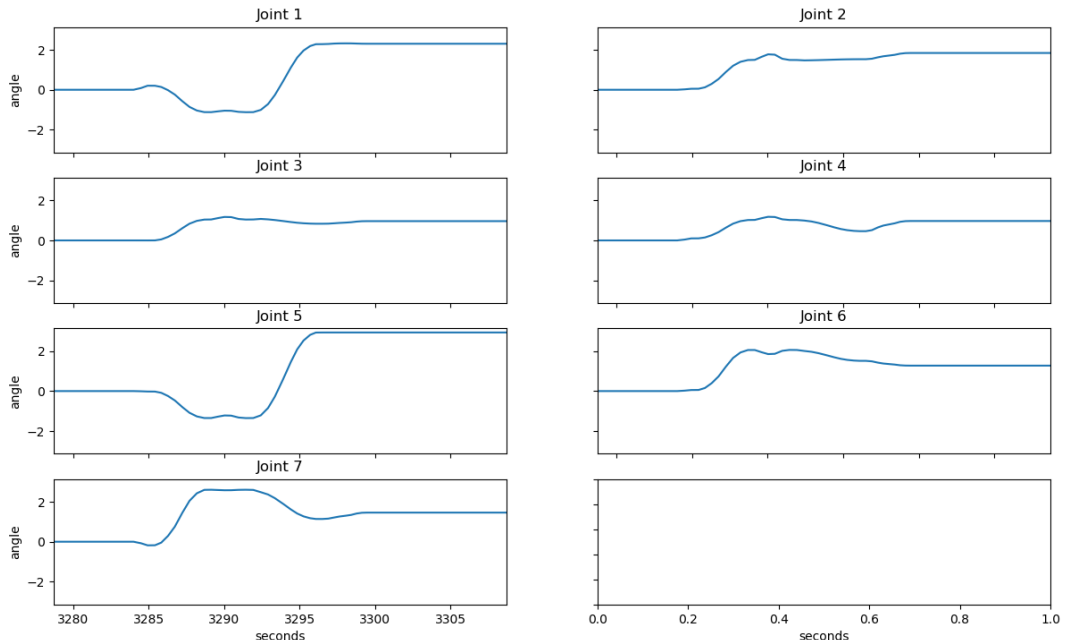


Figure 19: Trajectory diagrams in joints space.

8 Implementation with the ROS framework

8.1 Gazebo simulation environment

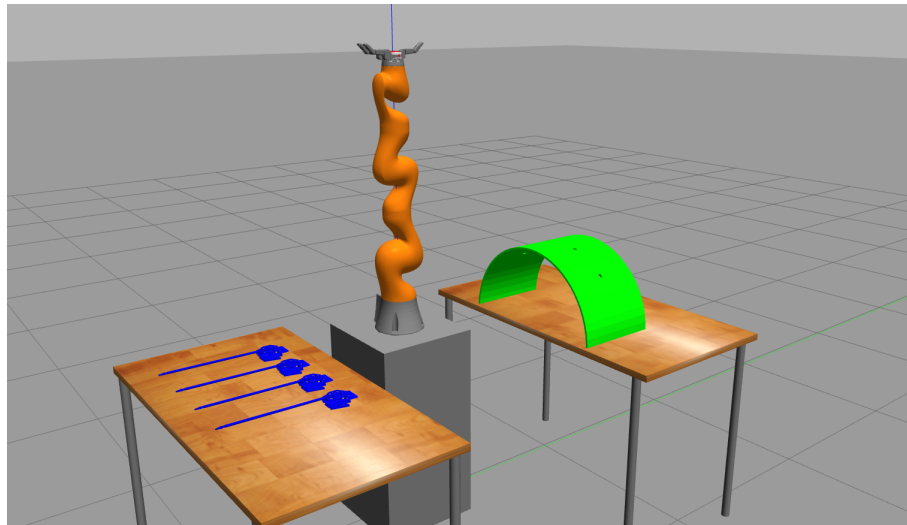


Figure 20: Simulation environment in Gazebo

The main environment setup of this thesis was designed using the Gazebo simulation environment and it consists of the following objects:

- the robot arm, KUKA®iiwa14 lbr, being at the center of the setup
- the robot base, so that the robot arm can better reach the tools and the surgical site and have more flexibility in movement
- 2 tables, one for the tools and one for the surgical site
- 4 surgical tools, using a modified version of the surgical tools used in the Raven II surgical platform
- a mounting dock, which has holes that have the same role as the trocars (small tubes from which the surgical tool is inserted). Initially a mounting dock with 4 same holes of 4mm diameter was used, but it was later replaced with a new one with holes of variable diameters to test feasibility of pivot motions. Larger diameters means more space for motion planner to search for solution and thus more probable to find a solution.

8.2 Visualization and Motion Planning with RViz and Moveit

Motion Planning parameters outside of body:

- Position tolerance: 50 μ m
- Orientation tolerance: 0.00005 deg
- Planning time: 10s

Motion Planning parameters inside of body:

- Position tolerance:
- Orientation tolerance:

- Planning time
- End-effector interpolation step: 1mm
- Maximum velocity scaling factor

Sometimes the motion planner finds a solution but the execution from the controller is aborted. After many iterations of the same experiment this does not happen always, which means that the feasibility of the execution of the movement by the controller depends on the initial state of the robot, i.e. if initially some joints of the robot are at their boundaries, then the next commanded trajectory maybe unfeasible.

At each time step it is important to publish a custom message containing all the information about the kinematic state of the robot. In this thesis a custom **ROS** message was created containing a tf transform with a 3D vector for the position and a quaternion for the rotation and a custom 6-by-7 matrix containing the values of the Jacobian. The MoveIt library, from which the kinematic state of the robot is obtained, returns the orientation of the end effector as a 3-by-3 rotation matrix, but in the ROS tf message it must be expressed as a quaternion. To convert the matrix to a quaternion we first calculate the euler angles and then use these values to construct the quaternion “vector”. The quaternion representation of rotation is often preferred in robotic applications due to its efficiency in calculations and memory. To convert the transformation matrix to euler angles and then to quaternions the following formulas were used:

$$T = \begin{bmatrix} r_{11} & r_{12} & r_{13} & x \\ r_{21} & r_{22} & r_{23} & y \\ r_{31} & r_{32} & r_{33} & z \\ 0 & 0 & 0 & 1 \end{bmatrix}$$

$$\varphi = \text{atan2}(r_{21}, r_{11})$$

$$\theta = \text{atan2}(-r_{31}, \sqrt{r_{11}^2 + r_{21}^2})$$

$$\psi = \text{atan2}(r_{32}, r_{33})$$

where T is the transformation matrix and φ, θ, ψ are the roll, pitch and yaw (Euler) angles.

8.3 Experiments and Development methodology

- 8.3.1 Robot Planner 1
- 8.3.2 Robot Planner 2
- 8.3.3 Robot Planner 3
- 8.3.4 Robot Planner 4
- 8.3.5 Robot Planner 5

9 Results and Future Work

- 9.1 Results
- 9.2 Conclusions & Comparison with similar projects
- 9.3 Future Work

Nomenclature

$\hat{\mathbf{r}}, \hat{\boldsymbol{\theta}}, \hat{\boldsymbol{\phi}}$ Unit vectors of r, θ, φ axes respectively, in spherical coordinates

$\hat{\mathbf{x}}, \hat{\mathbf{y}}, \hat{\mathbf{z}}$ Unit vectors of x, y, z axes respectively

\mathcal{L}_q Dexterity measure of the robotic arm

\mathcal{M} Manipulability measure of the robotic arm

${}^{i-1}\mathbf{p}_{iO}$ Position vector from the origin of the coordinate frame $\{i\}$ to the origin of the coordinate frame $\{i - 1\}$

${}^{i-1}R_i$ Rotation matrix from coordinate frame $\{i\}$ to coordinate frame $\{i - 1\}$

${}^{i-1}T_i$ Transformation matrix from coordinate frame $\{i\}$ to coordinate frame $\{i - 1\}$

c_i Shorthand notation for $\cos\theta_i$

J^\dagger Pseudoinverse of the Jacobian

s_i Shorthand notation for $\sin\theta_i$

List of Figures

1	The PUMA 560 robotic arm, which was the first to be used in surgery robotics in 1985	10
2	DaVinci Xi Patient Cart	11
3	DaVinci Xi Surgeon Console	12
4	Joint reference frames of the KUKA iiwa14 robot	13
5	Calculation of angles θ_2, θ_4	14
6	KUKA iiwa LBR14 workspace dimensions	15
7	Barrett Hand gripper (model BH8-282) dimensions	16
8	Force control on a Barrett Hand gripper finger	17
9	Simple tool detection in simulation based on color, using OpenCV. The green polygon is the convex hull, and the red point is the estimated center of mass	17
10	Disparity image calculated from the 2 cameras	18
11	Point cloud of surgical tools, generated from the 2 cameras and visualized in RViz	18
12	Estimation of tool's pose (position and orientation)	19
13	Simple trocar detection in simulation based on color, using OpenCV. In simulation, the trocar is simply considered to be a small cylindrical hole and it's center is the fulcrum point	19
14	Tool pose at target point B calculated with respect to Fulcrum's reference frame $\{F\}$	20
15	Circular trajectory of tool tip with respect to Fulcrum reference frame	21
16	Line segment trajectory of tool tip with respect to Fulcrum reference frame	22
17	Plot the manipulability of the robot arm at sample points of the executed trajectory	23
18	Circular trajectory around the z axis of the home position of the robot	24
19	Trajectory diagrams in joints space.	24
20	Simulation environment in Gazebo	25

List of programs

Bibliography

- [1] E. Bauzano et al. "Active wrists endoscope navigation in robotized laparoscopic surgery". In: *2009 IEEE International Conference on Mechatronics*. Apr. 2009, pp. 1–6. doi: 10.1109/ICMECH.2009.4957177.
- [2] M. C. Capolei et al. "Positioning the laparoscopic camera with industrial robot arm". In: *2017 3rd International Conference on Control, Automation and Robotics (ICCAR)*. Apr. 2017, pp. 138–143. doi: 10.1109/ICCAR.2017.7942675.
- [3] Sachin Chitta et al. "ros_control: A generic and simple control framework for ROS". In: *The Journal of Open Source Software* (2017). doi: 10.21105/joss.00456. URL: <http://www.theoj.org/joss-papers/joss.00456/10.21105.joss.00456.pdf>.
- [4] G. Cowley. "Introducing "Robodoc". A robot finds his calling—in the operating room". In: *Newsweek* 120.21 (Nov. 1992), p. 86.
- [5] Carlos Faria et al. "Position-based kinematics for 7-DoF serial manipulators with global configuration control, joint limit and singularity avoidance". In: *Mechanism and Machine Theory* 121 (2018), pp. 317–334. ISSN: 0094-114X. doi: <https://doi.org/10.1016/j.mechmachtheory.2017.10.025>. URL: <http://www.sciencedirect.com/science/article/pii/S0094114X17306559>.
- [6] Tully Foote. "tf: The transform library". In: *Technologies for Practical Robot Applications (TePRA), 2013 IEEE International Conference on*. Open-Source Software workshop. Apr. 2013, pp. 1–6. doi: 10.1109/TePRA.2013.6556373.
- [7] K. Fujii et al. "Gaze contingent cartesian control of a robotic arm for laparoscopic surgery". In: *2013 IEEE/RSJ International Conference on Intelligent Robots and Systems*. Nov. 2013, pp. 3582–3589. doi: 10.1109/IROS.2013.6696867.

- [8] M. Fujii et al. "Relationship between workspace reduction due to collisions and distance between endoscope and target organ in pediatric endoscopic surgery". In: *5th IEEE RAS/EMBS International Conference on Biomedical Robotics and Biomechatronics*. Aug. 2014, pp. 46–51. DOI: 10.1109/BIOROB.2014.6913750.
- [9] J. Funda et al. "Control and evaluation of a 7-axis surgical robot for laparoscopy". In: *Proceedings of 1995 IEEE International Conference on Robotics and Automation*. Vol. 2. 1995, 1477–1484 vol.2.
- [10] G. Gras et al. "Implicit gaze-assisted adaptive motion scaling for highly articulated instrument manipulation". In: *2017 IEEE International Conference on Robotics and Automation (ICRA)*. May 2017, pp. 4233–4239. DOI: 10.1109/ICRA.2017.7989488.
- [11] Techbriefs Media Group. *Surgical Robotics: The Evolution of a Medical Technology - Medical Design Briefs*. URL: <https://www.medicaldesignbriefs.com/component/content/article/mdb/features/technology-leaders/25006> (visited on 09/18/2020).
- [12] G. B. Hanna, S. Shimi, and A. Cuschieri. "Optimal port locations for endoscopic intracorporeal knotting". In: *Surgical Endoscop* 11.4 (Apr. 1997), pp. 397–401. ISSN: 1432-2218. DOI: 10.1007/s004649900374. URL: <https://doi.org/10.1007/s004649900374>.
- [13] B. Hannaford et al. "Raven-II: An Open Platform for Surgical Robotics Research". In: *IEEE Transactions on Biomedical Engineering* 60.4 (Apr. 2013), pp. 954–959. ISSN: 1558-2531. DOI: 10.1109/TBME.2012.2228858.
- [14] M. R. Hasan et al. "Modelling and Control of the Barrett Hand for Grasping". In: *2013 UKSim 15th International Conference on Computer Modelling and Simulation*. Apr. 2013, pp. 230–235. DOI: 10.1109/UKSim.2013.142.
- [15] Felix C. Huang et al. "Learning kinematic mappings in laparoscopic surgery". In: *Conference proceedings : ... Annual International Conference of the IEEE Engineering in Medicine and Biology Society. IEEE Engineering in Medicine and Biology Society. Annual Conference 2010* (2010). PMC3280950[pmcid], pp. 2097–2102. ISSN: 1557-170X. DOI: 10.1109/IEMBS.2010.5626188. URL: <https://pubmed.ncbi.nlm.nih.gov/21095685>.
- [16] J. Hutzl and H. Wörn. "Spatial probability distribution for port planning in minimal invasive robotic surgery (MIRS)". In: *2015 6th International Conference on Automation, Robotics and Applications (ICARA)*. Feb. 2015, pp. 204–210. DOI: 10.1109/ICARA.2015.7081148.
- [17] Reza N. Jazar. *Theory of Applied Robotics, Kinematics, Dynamics, and Control (2nd Edition)*. Springer, Boston, MA, 2010. ISBN: 978-1-4419-1750-8. DOI: 10.1007/978-1-4419-1750-8.
- [18] I. Kuhlemann et al. "Robust inverse kinematics by configuration control for redundant manipulators with seven DoF". In: *2016 2nd International Conference on Control, Automation and Robotics (ICCAR)*. Apr. 2016, pp. 49–55. DOI: 10.1109/ICCAR.2016.7486697.
- [19] Kevin M Lynch and Frank C. Park. *Modern Robotics: Mechanics, Planning, and Control*. English (US). Cambridge Univeristy Press, 2017. ISBN: 978-1107156302.
- [20] Q. Mei et al. "PROBOT — A computer integrated prostatectomy system". In: *Visualization in Biomedical Computing*. Ed. by Karl Heinz Höhne and Ron Kikinis. Berlin, Heidelberg: Springer Berlin Heidelberg, 1996, pp. 581–590. ISBN: 978-3-540-70739-4.
- [21] Victor F. Muñoz et al. "Pivoting motion control for a laparoscopic assistant robot and human clinical trials". In: *Advanced Robotics* 19 (2005), pp. 694–712.
- [22] A. A. Navarro et al. "Automatic positioning of surgical instruments in minimally invasive robotic surgery through vision-based motion analysis". In: *2007 IEEE/RSJ International Conference on Intelligent Robots and Systems*. Oct. 2007, pp. 202–207. DOI: 10.1109/IROS.2007.4399150.
- [23] Jason M. O'Kane. *A Gentle Introduction to ROS*. Available at <http://www.cse.sc.edu/~jokane/agitr/>. Independently published, Oct. 2013. ISBN: 978-1492143239.
- [24] Jaydeep Palep. "Robotic assisted minimally invasive surgery". In: *Journal of minimal access surgery* 5 (Feb. 2009), pp. 1–7. DOI: 10.4103/0972-9941.51313.

- [25] Morgan Quigley et al. “ROS: an open-source Robot Operating System”. In: *ICRA Workshop on Open Source Software*. 2009.
- [26] H. Shao et al. “A New CT-Aided Robotic Stereotaxis System”. In: 1985.
- [27] I. A. Sucan and S. Chitta. *Moveit!* URL: <https://moveit.ros.org/> (visited on 04/28/2020).
- [28] Go Watanabe, ed. *Robotic Surgery*. Springer Japan, 2014. doi: 10.1007/978-4-431-54853-9. URL: <https://doi.org/10.1007/978-4-431-54853-9>.
- [29] Haiwang Xu et al. “Laparoscopic Robot Design and Kinematic Validation”. In: Jan. 2007, pp. 1426–1431. doi: 10.1109/ROBIO.2006.340138.
- [30] Tao Yang et al. “Mechanism of a Learning Robot Manipulator for Laparoscopic Surgical Training”. In: *Intelligent Autonomous Systems 12*. Ed. by Sukhan Lee et al. Berlin, Heidelberg: Springer Berlin Heidelberg, 2013, pp. 17–26. ISBN: 978-3-642-33932-5.
- [31] L. Yu et al. “Research on the Trajectory Planning of the Minimally Invasive Surgical Robot 6-DOF Manipulator”. In: *2010 International Conference on Biomedical Engineering and Computer Science*. Apr. 2010, pp. 1–4. doi: 10.1109/ICBECS.2010.5462451.